

The Wendelstein Calar Alto Pixellensing Project (WeCAPP): the M31 Nova catalogue

C.-H. Lee¹, A. Riffeser¹, S. Seitz^{1,2}, R. Bender^{1,2}, J. Fliri³, U. Hopp^{1,2}, C. Ries¹, O. Bärbantner¹, and
C. Gössl¹

¹ University Observatory Munich, Scheinerstrasse 1, 81679 München, Germany

² Max Planck Institute for Extraterrestrial Physics, Giessenbachstrasse, 85748 Garching, Germany

³ GEPI, CNRS UMR 8111, Observatoire de Paris, 92195 Meudon, France

Received / Accepted

ABSTRACT

We present light curves from the novae detected in the long-term, M31 monitoring WeCAPP project. The goal of WeCAPP is to constrain the compact dark matter fraction of the M31 halo with microlensing observations. As a by product we have detected 91 novae benefiting from the high cadence and highly sensitive difference imaging technique required for pixellensing. We thus can now present the largest CCD and optical filters based nova light curve sample up-to-date towards M31. We also obtained thorough coverage of the light curve before and after the eruption thanks to the long-term monitoring. We apply the nova taxonomy proposed by Strope et al. (2010) to our nova candidates and found 29 S-class novae, 10 C-class novae, 2 O-class novae and 1 J-class nova. We have investigated the universal decline law advocated by Hachichu and Kato (2006) on the S-class novae. In addition, we correlated our catalogue with the literature and found 4 potential recurrent novae. Part of our catalogue has been used to search for optical counter-parts of the super soft X-ray sources detected in M31 (Pietsch et al. 2005). Optical surveys like WeCAPP, and coordinated with multi-wavelength observation, will continue to shed light on the underlying physical mechanism of novae in the future.

Key words. Stars: nova, cataclysmic Variable - Galaxies: individual: M31

1. Introduction

Classical novae span a subclass of cataclysmic variables, consisting of a white dwarf which interacts with a late-type companion star. The companion loses its mass through Roche lobe overflow, forming an accretion disk around the white dwarf. The mass transfer from the companion induces thermo-nuclear runaway (TNR) onto the surface of the white dwarf, which leads to the nova eruption.

Novae are important in several aspects. First of all, they have the potential to serve as standard candles of extragalactic distance indication. This is due to the relation between the maximum luminosity of the light curve and the rate of decline. Hubble (1929) first noticed that brighter novae are prone to steeper decline. The empirical ‘Maximum Magnitude versus Rate of Decline’ (MMRD) relation was further investigated by Zwicky (1936) and studied quantitatively by McLaughlin (1945) and Arp (1956). The theoretical foundation for MMRD relation is laid down by Shara (1981) and further revised by Livio (1992).

Novae could also shed light on the underlying stellar population of the environment. For example, della Valle & Livio (1995) proposed that fast novae ($t_2 < 12$ days) are related to stars belonging to Population I with relatively massive white dwarfs, while slow novae are associated to Population II stars and have less massive white dwarfs.

In addition, novae play a role in the galactic abundances. Novae have been considered as major sources of galactic ^{13}C , ^{15}N and ^{17}O , and minor contributors to ^7Li , ^9F and ^{26}Al . However, novae hardly contribute to the overall galactic metallicity compared to supernovae or AGB stars, because only 10^{-4} to $10^{-5}M_{\odot}$ are ejected per nova outburst (José & Hernanz 2007).

Recurrent novae are also regarded as possible supernovae progenitor candidates (see e.g. Schaefer 2010, and reference therein.). The fundamental question is whether recurrent novae accumulate enough mass onto the central white dwarf envelope and turn into supernovae progenitors even after several novae explosions.

Last but not the least, novae are main contributors to the class of super soft X-ray sources (SSS). Pietsch et al. (2005) searched for X-ray counterparts of the optical novae in M31, and found that novae are major sources of soft X-ray emission. The SSS phase can provide us with information on the white dwarf mass, the ejected and burned mass in the outburst (e.g. Pietsch 2010).

Due to the interstellar extinction in the Galactic disk, we can only observe a small fraction of the Galactic novae that erupt each year (Shafter 1997). Thus, we need to take into account rather large (and likely uncertain) corrections for incompleteness when determining the spatial distribution or estimation of the Galactic nova rate. In such case, M31 is an ideal target for a novae survey because novae are still bright enough to be observed ($m_R < 20$ mag) and it

Send offprint requests to: chlee@usm.lmu.de

is possible to cover the entire M31 galaxy within several pointings.

Novae monitoring campaigns towards M31 can be dated back to the pioneering work done by Hubble in 1920s (Hubble 1929).

A list of all the campaigns with published novae in M31 that we are aware of is shown in Table 1, with most of the data compiled by Shafter & Irby (2001) and Darnley et al. (2004).

Despite the extensive search towards M31, most of previous studies have only sparse observations and thus make the analysis of nova light curve rather difficult. Our WeCAPP project is dedicated to monitoring M31 with up to 4 we categorize our nova candidates according to the classification scheme of Strobe et al. (2010). We apply the power-law decline proposed by Hachisu & Kato (2006) to fit the smooth class light curves in Sect. 4.1. Novae showing cusp, oscillation or jitter features in their light curves are presented in Sect. 4.2 - 4.4. We then correlate our nova candidates with literature to search for recurrent novae in Sect. 5 We show the rate of decline of your nova candidates and the distribution of their speed class in Sect. 6 and end the paper with the conclusions in Sect. 7. All the light curves in our catalogue are presented in the Appendix.

2. Observations and data reduction

The WeCAPP project (Riffeser et al. 2001) was a dedicated survey to search for microlensing events towards our neighboring galaxy M31. We continuously monitored the bulge of M31 (when it was visible, when the weather was cooperative and when there was an observer) between September 1997 and March 2008 using the 0.8 m telescope of the Wendelstein Observatory located in the Bavarian Alps. The data was taken optimally on a daily basis in both R and I filters with a field of view of $8'.3 \times 8'.3$. From June 1999 to February 2002 we further extended our observations with the 1.23 m ($17'.2 \times 17'.2$ FOV) telescope of the Calar Alto Observatory in Spain. After 2002 we use the Wendelstein telescope solely to mosaic the full Calar Alto field of view with four pointings. The position of these four pointing are indicated in Fig. 1.

The data volume and quality of the four pointings (F1, F2, F3, F4) drastically differs during the 11 seasons. A list of the number of nights observed in each season is shown in Table 2. A detailed overview of the observations can be found in Fliri et al. (2006) and Riffeser et. al. (in prep.).

To quantify a realistic time sampling of the survey we define “good quality data points” as data points with PSF fluxes with an error below 0.4×10^{-5} Jy. In Fig. 2 we show for every night the fractional area of pixels with errors below this limit. 0% indicates we have no observations during the night.

Fig. 3 shows the spatial variation of the fraction of all data with flux errors below the flux error limit averaged over 11 seasons. It demonstrates that we expect most of our novae in field F1 and fewer in the fields F2, F3, and F4. The field F1 was observed much more frequently than the other one because it is the subfield with highest lensing probability.

The data was then reduced by our customized pipeline MUPIPE (see Gössl & Riffeser 2002), which performs CCD reduction, position alignment, photometric align-

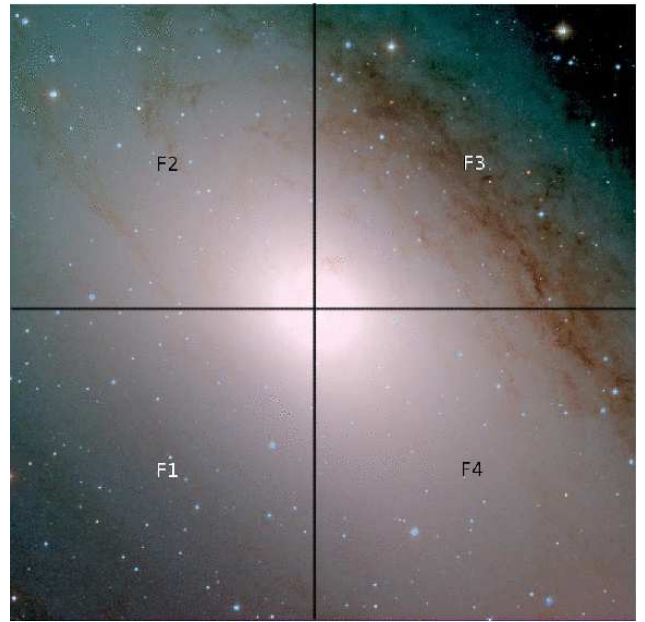


Fig. 1. M31 composite image (V -, R -, and I -band) taken at the Calar Alto Observatory. The black lines mark the four pointings (F1 to F4) from the Wendelstein Observatory to mosaic the full FOV of the Calar Alto Observatory.

Table 2. Lists of the analyzed nights per season from the 11-year WeCAPP campaign

season	R -band				I -band			
	F1	F2	F3	F4	F1	F2	F3	F4
1997 - 1998	36	7	1	4	33	7	0	3
1998 - 1999	33	1	1	1	28	1	1	1
1999 - 2000	154	0	0	0	145	0	0	0
2000 - 2001	184	108	124	108	159	89	104	89
2001 - 2002	240	136	159	136	212	119	140	119
2002 - 2003	34	18	24	18	30	16	24	18
2003 - 2004	35	24	29	31	33	21	26	29
2004 - 2005	25	23	26	25	19	16	19	19
2005 - 2006	30	26	28	29	26	20	22	23
2006 - 2007	107	106	103	103	48	45	46	47
2007 - 2008	62	56	52	58	36	35	35	38
total	940	505	547	513	769	369	417	386

Notes. Each season starts from the 1st of May until the 30th of April in the next year. The WeCAPP campaigns began in 1997 focusing on F1 with the Wendelstein Observatory. From 1999 until 2002 we extended our observations by including the Calar Alto Observatory, which boosted the number of images taken in these seasons. From 2002 on, we use the Wendelstein Observatory solely and mosaic the full Calar Alto FOV with four pointings.

ment, frame stacking and difference imaging following the algorithm of Alard & Lupton (1998).

After the difference imaging, we perform PSF photometry on each pixel as follows. First, we extracted the PSF from several isolated, bright and unsaturated reference stars. Then we fit this PSF to all variable sources. Finally, we integrate the count rates over the area of the PSF to determine the flux of the source.

The results of the project are presented in Riffeser et al. (2003, 2008) and partially contributed

Table 1. Principal M31 classical nova surveys

Author(s)/Project	Epoch	Filter(s)	Detector	Novae	Annual rate	Reference(s)
Hubble	1909–1927	B	Plates	85	~ 30	Hubble (1929)
Arp	1953–1954	B	Plates	30	26 ± 4	Arp (1956)
Rosino <i>et al.</i>	1955–1986	B	Plates	142	-	Rosino (1964, 1973); Rosino <i>et al.</i> (1989)
Ciardullo <i>et al.</i>	1982–1986	B, H α	CCD	40	-	Ciardullo <i>et al.</i> (1987, 1990)
Sharov & Alksins	1969–1989	B	Plates	21	-	Sharov & Alksnis (1991)
Tomaney & Shafter	1987–1989	H α	CCD	9	-	Tomaney & Shafter (1992)
Shafter & Irby	1990–1997	H α	CCD	72	37^{+12}_{-8}	Shafter & Irby (2001)
Rector <i>et al.</i>	1995–1999	H α	CCD	44	-	Rector <i>et al.</i> (1999b)
AGAPE	1994–1996	R, I	CCD	12	-	Ansari <i>et al.</i> (2004)
POINT-AGAPE	1999–2002	r', i', g'	CCD	20	65^{+16}_{-15}	Darnley <i>et al.</i> (2006)
NMS	2001–2002	R, I	CCD	2	-	Joshi <i>et al.</i> (2004)
WeCAPP	1997–2008	R, I	CCD	91	-	This work

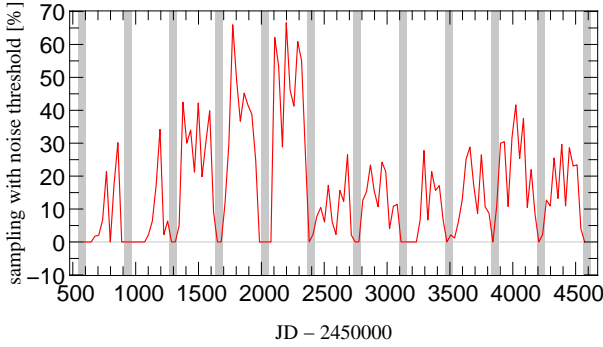


Fig. 2. Fraction of good quality data points in t averaged over the survey area. The definition of good quality is given in the text. The vertical grey zones indicate the time when M31 is not observable from the location of the telescopes during May and June). 0% indicates we have no observations during the night.

to Calchi Novati *et al.* (2010). In addition to the original microlensing targets, the intensive observations in two bands also yields more than 20,000 variables in the bulge of M31 (Fliri *et al.* 2006) and the nova candidates presented in this paper.

3. Nova detection

To establish an automatic detection for nova candidates, we apply the following criteria for candidates selection based on the measured R -band PSF flux (as mentioned in Sect. 2):

- The significance for variability must be 10σ relative to the baseline and the measured flux excess of the variable source must be a local maximum around neighbouring pixels at a given time step. Note that σ throughout this paper refers to the errors of the individual PSF flux excess measurements.
- The variable source must have a measured flux excess larger than 4×10^{-5} Jy in R -band (corresponding to $m_R = -2.5 \log(\frac{4 \times 10^{-5} \text{ Jy}}{F_{\text{Vega}, R}}) \sim 19.7$ mag, with $F_{\text{Vega}, R} = 3060$ Jy being the flux of Vega in the R -band) and the first measurement after the measured maximum flux excess must have a flux excess $> 2 \times 10^{-5}$ Jy.

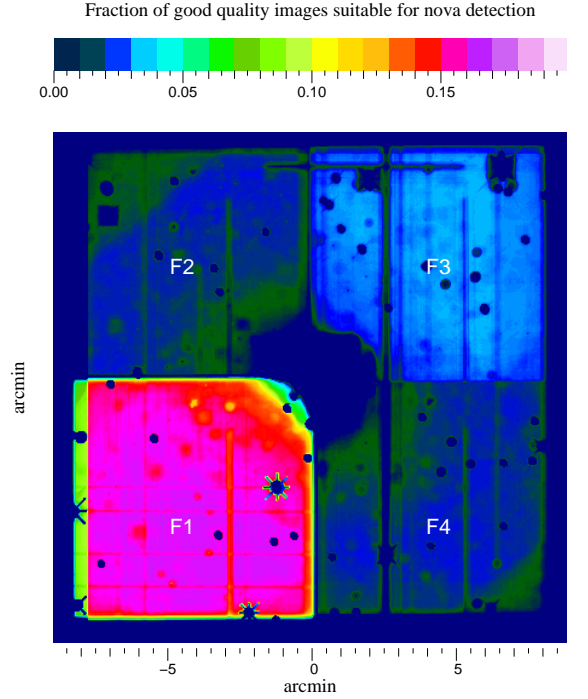


Fig. 3. Fraction of good quality data points in (x, y) averaged over time t . The definition of good quality is given in the text. The low fraction in the central part is caused by the high noise of M31 itself.

- To use the eruptive nature of novae, we define the strength s of the outburst:

$$s = \frac{\Delta F_{\text{max}}/\sigma_{\text{max}}^2 + \Delta F_{\text{max}+1}/\sigma_{\text{max}+1}^2}{1/\sigma_{\text{max}}^2 + 1/\sigma_{\text{max}+1}^2} \quad (1)$$

where ΔF_{max} is the measured maximum flux excess relative to the reference image and $\Delta F_{\text{max}+1}$ is the first measurement after the measured maximum flux excess. The σ_{max} and $\sigma_{\text{max}+1}$ are the errors in the measurements of the flux excess. We require $s > 4.6 \times 10^{-5}$ Jy nova detection.

- To avoid false contamination from periodically varying sources, we define the asymmetry a between positive and negative outliers in the light curve relative to the baseline:

$$a = \frac{\text{Number of data points with } \Delta F > 5\sigma}{\text{Number of data points with } \Delta F < -5\sigma} - 1. \quad (2)$$

Table 3. Detection criteria for nova candidates

Criterion	Number
Full light curves	4043256
Local flux maximum with $s > 4.6 \times 10^{-5}$ Jy and $a > 4.7$	1005
Masking of bright stars	156
Grouping	105
Inspection by eye	91

This quantity a is useful in filtering out normal variable sources, which have $a \sim 0$, while the eruptive nature of novae lead to $a \gg 1$. We empirically require a to be larger than 4.7 to be suitable for nova detection.

- We then apply a special mask to filter false detections around bright stars, especially spikes.
- After the masking, we apply a group algorithm to find multiple pixel detections connecting to the same nova candidate in different time steps.
- In the last step, we inspect the difference images and light curves by eye to make sure that no image artefact escapes our detection and is misinterpreted as a nova.

We combine the criteria 1-4 into one single step. The detections filtered out by each steps are shown in Table 3.

Among the nova candidates, 24 are discovered by WeCAPP project for the first time, while 5 of them are known but were not officially published and can be found on the CBAT¹ or Extragalactic Novae² webpages. The rest of the nova candidates are published and can be found in the literature, see e.g. Pietsch et al. (2007); Pietsch (2010)³. The positions and light curves of these 91 novae are presented in Table 4 and in the Appendix.

4. Nova taxonomy

Although all novae slightly differ, it is possible to group novae by their light-curve or spectroscopic properties. One of the commonly used methods to characterize novae is the ‘speed class’ proposed by Payne-Gaposchkin (1964), who categorized novae according to their light-curve evolution and described the decline time-scale by the time needed to drop by 2 magnitudes below the maximum (t_2). Williams (1992) did a thorough study of the spectroscopic properties of the novae, and categorized novae into Fe (galactic thick disk novae) or He (galactic disk novae) group according to the most prominent features in their spectra. Della Valle & Livio (1998) further established the connection between the speed class and spectroscopic classification. They found that fast novae are mainly related to the He novae, while the slow novae tend to show Fe II features in their spectra. The proposed explanation behind is that He novae are from the galactic disk and prone to have massive white dwarfs, thus having fast and steep decline. On the other hand, the Fe II novae originate from the less massive population II stars in the galactic thick disk, and hence have a slow decline.

¹ M31 (Apparent) Novae Page, http://www.cfa.harvard.edu/iau/CBAT_M31.html

² www.rochesterastronomy.org/novae.html

³ An up-to-date online-version of the catalog can be found at <http://www.mpe.mpg.de/~m31novae/opt/m31/index.php>

The speed class is not enough to fully account for the differences between novae. Strobe et al. (2010) gathered 93 galactic novae from the American Association of Variable Star Observers (AAVSO) and made a thorough study using the complete coverage of their light curves.

They suggested to classify the novae according to their distinct features during their decline, such as the plateau, the cusp by the secondary brightening and the dip by the dust.

In this section we classify our nova candidates (if possible) following the taxonomy proposed by Strobe et al. (2010). Readers are referred to Table 3 and Figure 2 in Strobe et al. (2010) for the definition and exemplary light curves for different nova classes. Note that the classification scheme of Strobe et al. (2010) is based on the V -band magnitude, while we are using R -band and might be affected by the strong $H\alpha$ emission. We thus check our I -band light curve, which does not affected by the strong $H\alpha$ emission, and identify the apparent features in the nova classification scheme of Strobe et al. (2010) in both R and I -band.

4.1. S Class and the universal decline law

The S-class novae have smooth light curves following the universal power-law decline ($F \propto t^{-1.75}$) due to free-free emission expanding shell as proposed by Hachisu & Kato (2006). In principle, the classification scheme of Strobe et al. (2010) is based on the fact that all the light curves originate from the S-class. The S-class is indeed consistent to the vast majority of our nova candidates. To verify the universal decline law, we thus fit our candidate light curves with a 4-parameter formula:

$$\Delta F = f_b + f_0 \times (t - t_0)^\alpha, \quad (3)$$

where f_b is the baseline level and will be different from zero in cases where the nova candidate flux is present in the reference frame used in difference imaging or there is a variable close to it (see e.g. the light curve of WeCAPP-N10 in the appendix). f_0 gives the proportional factor between the flux and time, t_0 is the onset of nova outburst and α is the index of the power-law decline. After the first iteration, we found that some candidates have unreasonable t_0 long before the nova eruption. For such events, we use a 5-parameter formula

$$\Delta F = f_b + f_0 \times (t - t_0)^\alpha, \quad t_0 \equiv t_{-1} + \delta^2 \quad (4)$$

with t_{-1} fixed at the last data point in the baseline just before the eruption to avoid unreasonable t_0 . The best-fit parameters for equations (3) and (4) are given in Table 5.

For the S-class nova, we first tried to fit the power-law decline for all the nova candidates. A candidate is classified as S-class nova only when the fitting routine finds a solution for either equation 3 or equation 4. N01, N09, N17, N24, N41, N49, N54, N58 and N77 are not attributed to S-class because the fitting routine failed to find a solution.

Our best-fit value of α from Table 5 for free t_0 solely and combined with fixed t_0 are -1.51 and -1.32 , respectively.

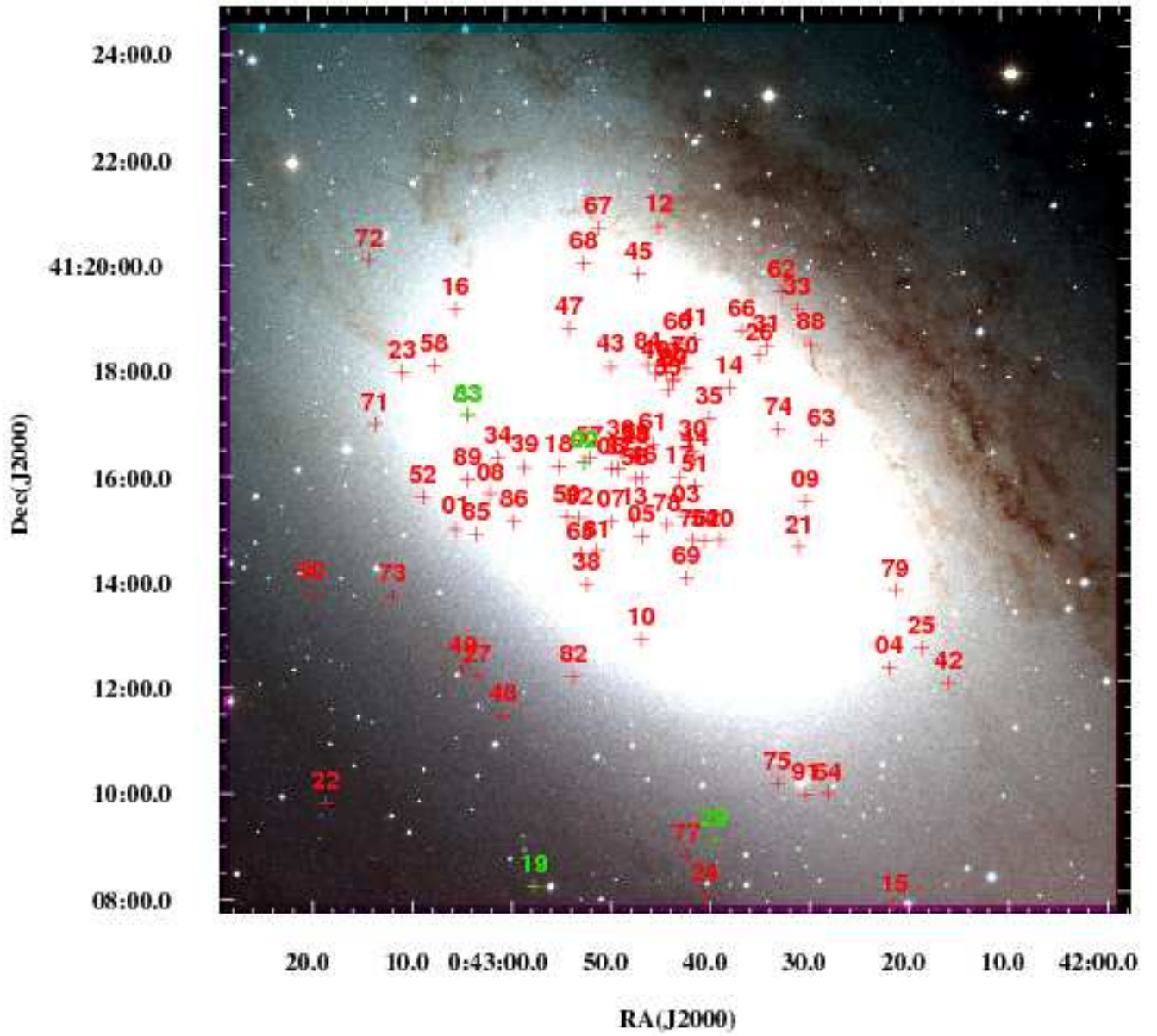


Fig. 4. Distribution of the WeCAPP nova candidates. The recurrent nova candidates (see Sect. 5) are marked in green. The overlaying image is a three-color-combined image using the observations obtained from Calar Alto observatories in V , R and I -band. The image has a size of $17'.2 \times 17'.2$.

Table 4. WeCAPP nova catalogue

Name	RA(2000) [h:m:s]	Dec(2000) [d:m:s]	t_{\max}	Δt_{\max} [day]	Class	CBAT	Discovery (and light curve) reference(s)	X-ray obs.	Spectroscopic obs.
N01	00:43:05.37	41:14:59.2	745.52	29.01	Unclassified	1997-10e	1997-14 in Shafter & Irby (2001)		
N02	00:42:52.35	41:16:13.2	750.45	33.95	Unclassified	1997-10f	1997-10 in Shafter & Irby (2001)		
N03	00:42:42.13	41:15:10.4	753.55	37.05	Unclassified	1997-11a	1997-07 in Shafter & Irby (2001)	Pietsch et al. (2007) Henze et al. (2010a,b)	
N04	00:42:21.76	41:12:16.2	753.55	37.05	Unclassified	1997-10c	1997-02 in Shafter & Irby (2001)		
N05	00:42:46.64	41:14:49.2	1109.48	243.19	Unclassified	1998-09d	IAUC 7015, Sharov et al. (2000)		Fe II, Shafter et al. (2011b)
N06	00:42:49.65	41:16:06.5	1251.30	2.00	Unclassified	1999-02a	This work		
N07	00:42:49.69	41:15:05.6	1359.55	0.93	Cusp	1999-06a	IAUC 7218, PAV-78668 in An et al. (2004)		Fe II, Shafter et al. (2011b)
N08	00:43:01.85	41:15:38.4	1372.62	1.01	Smooth	1999-06b	Rector et al. (1999a)		
N09	00:42:30.11	41:15:27.3	1719.62	553.15	Unclassified	2000-06a	This work		
N10	00:42:46.75	41:12:51.9	1726.63	1.00	Cusp	2000-08b	Pietsch et al. (2007)		
N11	00:42:43.97	41:17:55.5	1754.64	18.01	Oscillation	2000-07a	PACN-00-01 in Darnley et al. (2004)	Pietsch et al. (2005, 2007) Orio (2006)	
N12	00:42:44.65	41:20:40.6	1755.65	1.02	Cusp	2000-07b	PACN-00-03 in Darnley et al. (2004)		
N13	00:42:47.45	41:15:07.8	1763.66	1.02	Cusp	2000-08a	Pietsch et al. (2007)	Pietsch et al. (2005, 2007)	
N14	00:42:37.70	41:17:37.8	1766.64	1.00	Cusp	2000-08d	PACN-00-04 in Darnley et al. (2004)		
N15	00:42:21.49	41:07:47.3	1932.34	1.04	Cusp	2001-01a	This work	Henze et al. (2010a,b)	
N16	00:43:05.26	41:19:08.2	1948.34	4.02	Unclassified	2001-01b	This work		
N17	00:42:42.82	41:15:55.2	1940.33	6.04	Unclassified	2001-01c	This work		
N18	00:42:54.95	41:16:09.2	1948.34	4.02	Unclassified	2001-02a	This work		
N19	00:42:57.75	41:08:12.3	2097.56	124.25	Unclassified	2001-07b	This work		
N20	00:42:38.76	41:14:44.4	2097.56	124.25	Unclassified	2001-07c	This work		
N21	00:42:30.79	41:14:36.1	2130.63	3.00	Unclassified	2001-07d	IAUC 7674, PACN-01-01 in Darnley et al. (2004)		
N22	00:43:18.62	41:09:49.0	2094.56	121.25	Smooth	2001-07a	PAV-74935 in An et al. (2004)	Pietsch et al. (2005, 2007)	
N23	00:43:10.62	41:17:58.0	2163.65	28.02	Unclassified	2001-08b	PACN-01-03 in Darnley et al. (2004)		
N24	00:42:40.60	41:07:59.9	2163.65	28.02	Unclassified	2001-08c	PACN-01-04 in Darnley et al. (2004)		
N25	00:42:18.52	41:12:39.3	2163.65	28.02	Unclassified	2001-08a	IAUC 7684, PACN-01-02 in Darnley et al. (2004)		
N26	00:42:34.62	41:18:13.0	2151.60	0.99	Smooth	2001-08d	IAUC 7709, PAC-26277 in An et al. (2004)	Pietsch et al. (2005, 2007)	
N27	00:43:03.31	41:12:11.5	2190.48	1.90	Jitter	2001-10a	IAUC 7729, PACN-01-06 in Darnley et al. (2004) NMS2 in Joshi et al. (2004)	Pietsch et al. (2007) Henze et al. (2010a,b)	Fe II, Shafter et al. (2011b)
N28	00:42:47.21	41:16:18.7	2197.32	0.98	Oscillation	2001-10c	This work		
N29	00:42:39.59	41:09:02.9	2299.32	2.99	Unclassified	2001-12b	This work		
N30	00:42:41.44	41:16:24.6	2266.30	0.92	Smooth	2001-12a	IAUC 7794		Fe II, Shafter et al. (2011b)

Table 4. WeCAPP nova catalogue continued.

Name	RA(2000) [h:m:s]	Dec(2000) [d:m:s]	t_{\max}	Δt_{\max} [day]	Class	CBAT	Discovery (and light curve) reference(s)	X-ray obs.	Spectroscopic obs.
N31	00:42:33.89	41:18:24.0	2282.31	6.02	Smooth	2002-01b	IAUC 7794, PAV-26285 in An et al. (2004)	Pietsch et al. (2005, 2007)	He/N, Shafter et al. (2011b)
N32	00:42:52.89	41:15:10.4	2283.30	0.99	Cusp	2002-01a	IAUC 7794, PAV-79136 in An et al. (2004)		
N33	00:42:30.74	41:19:05.9	2325.38	4.02	Smooth	2002-02a	This work		
N34	00:43:01.08	41:16:19.9	2476.54	13.00	Smooth	2002-07a	IAUC 7937, IAUC 7938		
N35	00:42:39.74	41:17:03.3	2521.57	38.01	Doubtful	2002-07b	This work		
N36	00:42:48.66	41:16:26.3	2573.63	26.07	Doubtful	2002-08b	This work		
N37	00:42:48.90	41:16:05.3	2661.25	6.82	Smooth	2003-01b	This work		
N38	00:42:52.24	41:13:54.5	2797.53	91.24	Doubtful	2003-01c	IAUC 8155		
N39	00:42:58.38	41:16:08.3	2797.53	91.24	Smooth	2003-06a	IAUC 8155		
N40	00:42:45.12	41:17:54.0	2820.50	21.94	Smooth	2003-06c	IAUC 8165		
N41	00:42:41.14	41:18:32.4	2832.56	12.05	Unclassified	2003-06d	IAUC 8165		
N42	00:42:15.85	41:11:59.9	2834.44	5.96	Smooth	2003-07b	IAUC 8165, N3 in Simon et al. (2005)		
N43	00:42:49.64	41:18:02.0	2867.53	6.11	Doubtful	2003-08a	IAUC 8210		
N44	00:42:41.20	41:16:16.0	2925.46	16.95	Unclassified	2003-08c	IAUC 8226	Henze et al. (2010b)	
N45	00:42:46.74	41:19:47.4	2931.30	22.96	Smooth	2003-09b	IAUC 8222, N5 in Simon et al. (2005)		
N46	00:42:46.45	41:15:55.6	2925.42	26.88	Unclassified	2003-10a	This work		
N47	00:42:53.78	41:18:46.2	2949.54	8.12	Unclassified	2003-11a	IAUC 8248	Pietsch et al. (2007) Henze et al. (2010a)	
N48	00:43:00.76	41:11:26.9	2978.22	6.86	Smooth	2003-11b	IAUC 8253	Pietsch et al. (2007) Henze et al. (2010a)	
N49	00:43:04.73	41:12:21.9	2992.32	7.02	Unclassified	2003-12a	IAUC 8262, N8 in Simon et al. (2005)	Pietsch et al. (2007)	
N50	00:42:54.14	41:15:12.2	2994.32	2.00	Smooth	2003-12b	IAUC 8262	Pietsch et al. (2007)	
N51	00:42:41.18	41:15:45.0	3006.24	52.88	Unclassified	2004-01b	This work	Pietsch et al. (2007) Henze et al. (2010b)	
N52	00:43:08.65	41:15:35.3	3039.29	38.95	Smooth	2004-01a	N9 in Simon et al. (2005)	Pietsch et al. (2007)	
N53	00:42:47.28	41:16:21.4	3039.29	52.81	Cusp	2004-02a	This work	Pietsch et al. (2007)	
N54	00:42:40.28	41:14:42.5	3254.44	193.14	Unclassified	2004-09a	IAUC 8404	Pietsch et al. (2007)	Fe II, Shafter et al. (2011b)
N55	00:42:43.90	41:17:35.0	3319.60	9.30	Doubtful	2004-07a	Pietsch et al. (2007)	Pietsch et al. (2007)	
N56	00:42:47.24	41:15:54.5	3291.45	7.92	Unclassified	2004-10b	Pietsch et al. (2007)	Pietsch et al. (2007)	
N57	00:42:51.84	41:16:18.2	3291.37	7.84	Unclassified	2004-10a	ATEL 346	Pietsch et al. (2007)	
N58	00:43:07.46	41:18:04.6	3319.49	15.13	Unclassified	2004-11b	Pietsch et al. (2007)	Pietsch et al. (2007) Henze et al. (2010a)	He/N, Shafter et al. (2011b)
N59	00:42:47.17	41:16:19.8	3319.49	15.13	Smooth	2004-11f	CBAT	Pietsch et al. (2007)	
N60	00:42:42.81	41:18:27.8	3319.60	9.30	Unclassified	2004-11a	Pietsch et al. (2007)	Pietsch et al. (2007)	Fe II, Shafter et al. (2011b)

Table 4. WeCAPP nova catalogue continued.

Name	RA(2000) [h:m:s]	Dec(2000) [d:m:s]	t_{\max}	Δt_{\max} [day]	Class	CBAT	Discovery (and light curve) reference(s)	X-ray obs.	Spectroscopic obs.
N61	00:42:45.47	41:16:33.2	3348.42	28.93	Unclassified	2004-11d	Pietsch et al. (2007)	Pietsch et al. (2007)	
N62	00:42:32.29	41:19:25.7	3346.36	25.92	Cusp	2004-11c	CBAT	Pietsch et al. (2007)	
N63	00:42:28.39	41:16:36.1	3382.36	4.09	Unclassified	2005-01a	Pietsch et al. (2007)	Pietsch et al. (2007)	Fe II, Shafter et al. (2011b)
N64	00:42:28.10	41:09:54.7	3381.36	21.03	Unclassified	2004-12a	ATEL 379	Pietsch et al. (2007)	
N65	00:42:52.79	41:14:28.8	3426.28	17.92	Smooth	2005-02a	ATEL 421	Pietsch et al. (2007) Henze et al. (2010a,b)	
N66	00:42:36.37	41:18:41.8	3427.38	1.03	Doubtful	2005-02b	This work		
N67	00:42:50.80	41:20:39.8	3592.47	100.43	Cusp	2005-07a	Pietsch et al. (2007)	Henze et al. (2010a)	Fe II, Shafter et al. (2011b)
N68	00:42:52.25	41:19:59.4	3635.37	15.94	Smooth	2005-09a	CBAT	Henze et al. (2010a)	Fe II, ATEL 850
N69	00:42:42.11	41:14:01.1	3635.59	9.30	Unclassified	2005-09d	This work	Henze et al. (2010a)	
N70	00:42:42.12	41:18:00.3	3661.54	1.17	Unclassified	2005-10b	ATEL 651	Henze et al. (2010a)	
N71	00:43:13.42	41:16:58.9	3863.57	50.27	Smooth	2006-04a	ATEL 805	Henze et al. (2010a,c)	
N72	00:43:13.93	41:20:05.5	3863.57	50.27	Smooth	2006-05a	This work	Henze et al. (2010a)	
N73	00:43:11.81	41:13:44.7	3880.53	2.98	Unclassified	2006-06a	This work	Henze et al. (2010a)	Fe II, ATEL 850
N74	00:42:32.77	41:16:49.1	3867.57	54.27	Unclassified	2006-06b	ATEL 829	Henze et al. (2010a,b)	
N75	00:42:33.17	41:10:06.8	3984.41	3.89	Smooth	2006-09a	Calchi Novati et al. (2007)	Henze et al. (2010a)	
N76	00:42:41.45	41:14:44.5	4000.42	8.92	Unclassified	2006-09b	ATEL 884	Henze et al. (2010a)	
N77	00:42:42.39	41:08:45.6	3999.40	4.98	Unclassified	2006-09c	ATEL 887, Shafter et al. (2011a)	Henze et al. (2010a,b)	Fe II, Shafter et al. (2011b)
N78	00:42:44.05	41:15:02.1	4096.47	1.09	Unclassified	2006-11b [†]	This work		
N79	00:42:21.08	41:13:45.4	4095.38	5.02	Smooth	2006-12a	This work	Henze et al. (2010a,b)	Fe II, Shafter et al. (2011b)
N80	00:42:43.22	41:17:48.4	4095.52	5.08	Unclassified	2006-12c	ATEL 973	Henze et al. (2010a,b)	
N81	00:42:51.15	41:14:33.5	4122.43	6.14	Unclassified	2007-01a	CBAT	Henze et al. (2010a,b)	
N82	00:42:53.61	41:12:09.9	4166.30	13.03	Smooth	2007-03a	CBAT	Henze et al. (2010a,b)	
N83	00:43:04.05	41:17:08.3	4296.48	24.96	Smooth	2007-07a	ATEL 1131	Henze et al. (2010b)	
N84	00:42:45.91	41:18:04.4	4297.50	1.01	Smooth	2007-07b	ATEL 1139	Henze et al. (2010b)	Fe II, ATEL 1186
N85	00:43:03.29	41:14:53.0	4307.48	9.02	Smooth	2007-07c	ATEL 1146	Henze et al. (2010b)	Hybrid or He/N, ATEL 1186
N86	00:42:59.49	41:15:06.6	4337.45	2.95	Unclassified	2007-07d	ATEL 1162	Henze et al. (2010b)	
N87	00:42:43.30	41:17:44.1	4314.55	15.01	Smooth	2007-07e	ATEL 1156	Henze et al. (2010b)	Fe II, ATEL 1186
N88	00:42:29.39	41:18:24.8	4356.49	16.92	Smooth	2007-08c	IAUC 7664, ATEL 1198	Henze et al. (2010b)	
N89	00:43:04.18	41:15:54.1	4425.30	14.81	Unclassified	2007-11c	ATEL 1275	Henze et al. (2010b)	Fe II, Shafter et al. (2011b)
N90	00:43:19.98	41:13:46.3	4444.61	18.35	Smooth	2007-12b	This work	ATEL 1360, ATEL 1647 Bode et al. (2009)	He/N, Shafter et al. (2011b)
N91	00:42:30.37	41:09:53.6	4508.27	0.98	Unclassified	2008-02a	ATEL 1380	Henze et al. (2010b)	

Notes. We show the position and the time of maximum flux (expressed in JD – 2450000) of the nova candidates in columns 2, 3 and 4. The uncertainty of the position is smaller than $0''.1$ (see Riffeser et. al., in prep.). The uncertainty in the time of maximum flux Δt_{\max} in column 5 is derived from the time difference between t_{\max} and the last measurement before t_{\max} . The light curve classification is shown in column 6, with 'unclassified' indicates those novae we are not able to classify and 'doubtful' indicates the novae are more similar to other variables than novae. In column 7 we give the corresponding CBAT nomenclature. Column 8 list the references for discovery (and light curves) in optical. The spectroscopic and X-ray observations are shown in column 9 and 10. The 24 novae without discovery references are newly discovered by WeCAPP. [†] We also detected M31N-2006-12d on the same position, which is possibly rebrightening of M31N-2006-11b given the short time difference.

The power-law index for a free t_0 is close to the value given by Hachisu & Kato (2006), while the value of α from a combination of both free and fixed t_0 deviates from -1.75 , which indicates that we might have missed the true eruption date for some of the novae. Note that we constrain the value of power-law index α from the R -band images, which are contaminated by the $H\alpha$ emission line and might differ from the universal power-law index from Hachisu & Kato (2006).

4.2. C Class

The light curves of C-class novae have cusp shape, which first follow a power-law decline, then rise steeply to a second maximum and finally have a sharp drop. The characteristic C-class light curve has a secondary maximum emerging between 1 to 8 months after the primary peak (Strope et al. 2010). Kato et al. (2009) found that C-class light curve can be well-fitted by an exponential component superimposed on the smooth decline. They further proposed that the cusps can originate from a secondary ejection and the break-out into the optically thick nova winds. Hachisu & Kato (2009) also connect the formation of the cusp shape to the input of the magnetic energy from rotating white dwarf. In addition, the sharp drop before the light curve returns to the power-law decline is attributed to the sudden formation of dust as proposed by Lynch et al. (2008). We have found in total 10 candidates showing cusp features in our WeCAPP catalog and show their light curves in Fig. 7.

4.3. O Class

The O-class light curve follows the S-class light curve, but with the exception that at a given time interval the light curve shows quasi-sinusoidal self-similar oscillations during the course of decline. It has been shown that the white dwarf of the O-class novae is both highly magnetic and massive (Strope et al. 2010). However, these can not be the only effect leading to oscillation because the nova V1500 Cyg in Strope et al. (2010) which fulfills these requirements but does not show oscillation. There have been many proposals for the mechanism of oscillation, but none of them have been compared to and verified by observation (see Sect. 4 in Strope et al. 2010). The oscillation starts generally around 3 mag below the peak, which indicates that we might have missed the peak in our nova candidates N11 and N28, where the light curves are shown in Fig. 8 and in the appendix. In Fig. 8 we show the two O-class candidates discovered during our observation campaign.

4.4. J Class

The characteristics of J-class novae are the jitters on top of the smooth decline. These jitters are symmetric and sharp-topped flares superposed on the base of S-class light curve, which is the major difference from the O-class novae, while the latter bears oscillations up and down the smooth decline. The jitter usually has variations with amplitude larger than half of a magnitude. Jitters do not occur in the late tail of the light curve and most of them occur within 3 mag below the peak. Strope et al. (2010) further propose for two subclasses according to the emergence of the jit-

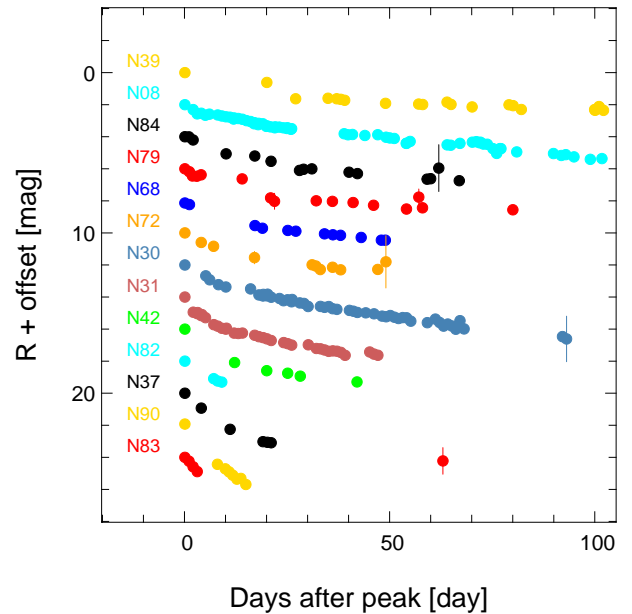


Fig. 5. S Class novae with free t_0 . The single offsets are -15.04 for N08, -3.59 for N30, -2.81 for N31, 2.84 for N37, -18.02 for N39, -0.88 for N42, -9.89 for N68, -8.06 for N72, -11.81 for N79 and 1.02 for N82, 5.14 for N83, -13.66 for N84 and 5.37 for N90 respectively. Note that for most of the data points the error bars are smaller than the symbol of the data points. Here we only show the decline part of the light curve. Full light curves can be found in the appendix.

ters: one subclass has jitters only near the peak, while the other has jitters spread all over the light curve roughly until the nova is 3 mag dimmer than the peak. Among our candidates we found one evident J-class light curve, which belongs to the second subclass of Strope et al. (2010) and is shown in Fig. 9.

It has been reported that there is a gradual increase of the time intervals between two successive jitters (Bianchini et al. 1992; Csák et al. 2005; Pejcha 2009; Tanaka et al. 2010), while Strope et al. (2010), using the same data set as Pejcha (2009), found no distinctive trend. We thus tried to search for such trend in our nova candidate N27 and performed a fitting with the following equation:

$$\log(t_J - t_{J-1}) = a \log(t_J - t_{max}) + b, \quad (5)$$

where t_J is the time of the J -th jitter.

The jitters used in the fitting are indicated by the vertical marks in Fig. 9. The time intervals between the successive jitters are shown in 10. Our best-fitted value is $a = 0.64 \pm 0.09$ and $b = 0.11 \pm 0.16$. The slope is smaller than the values of DK Lac ($a = 0.88$) and V4745 Sgr ($a = 0.79$) derived by Pejcha (2009) and $a = 0.79$ for the 6 novae presented by Tanaka et al. (2010). With only one J-class nova candidate in our catalog, we can not tell if this is a difference between the nova in M31 and Galactic novae, or it is simply a variation among individual novae.

4.5. Other classes

Besides the above-mentioned classes, there remains three more classes in the taxonomy of Strope et al. (2010):

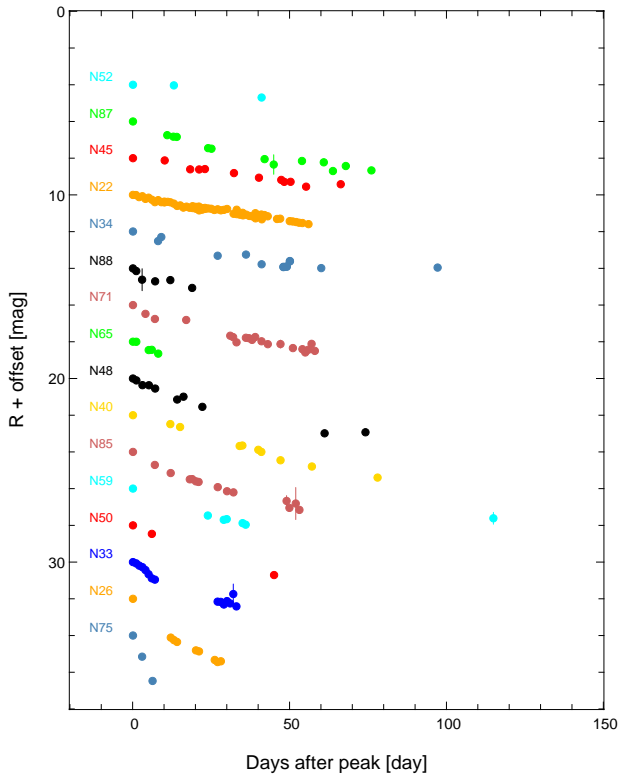


Fig. 6. S Class novae with fixed t_0 . The single offsets are -8.84 for N22, 15.17 for N26, 12.44 for N33, -6.44 for N34, 4.97 for N40, -10.40 for N45, 2.53 for N48, 10.92 for N50, -13.97 for N52, 8.05 for N59, -0.22 for N65, -1.84 for N71, 16.24 for N75, 6.70 for N85, -11.06 for N87 and -5.14 for N88 respectively. Here we only show the decline part of the light curve. Full light curves can be found in the appendix.

- Flat topped (F) class which has an extended interval at the peak with near constant brightness.
- Dust dip (D) class where the decline is interrupted by another very steep decline and followed by the recovery to just below the original decline.
- Plateau (P) class that the smooth decline is interrupted by a long-lasting and nearly flat interval, succeeded by the return to the original decline.

Among our candidates, however, we do not find evident light curves belonging to these classes. This could be partially attributed to the set-up of our observation campaign. For example, the dust dip for the extreme shallow dips in Strobe et al. (2010) occur more than 1 month after the peak, with the dip to be about 6 mag dimmer than the light curve maximum. Such magnitude variation can hardly be observed in M31, because it is too faint to be discerned. This implies that we might misclassified the D-class novae into other classes. The non-detection of the P-class novae can be explained by the filter system we used. Hachisu & Kato (2006) pointed out that the true plateau from the continuum radiation is best observed in the y -band filter. Since we are using the R and I -filter, it is possible that the plateau phase does not exist in the R and I -bands due to the influence of the emission lines during the course of decline.

To summarize, we have classified 42 nova candidates and find 69% to be S-class, 24% to be C-class, 5% to be O-class and 2% to be J-class, while Strobe et al. (2010) find

Table 5. Power-law decline fitting for s-class nova

Free t_0		
Name	$t_0(\text{JD}-2450000)$	α
N08	1337.9 ± 0.5	-2.07 ± 0.02
N30	2257.3 ± 0.1	-1.55 ± 0.01
N31	2277.9 ± 0.2	-1.29 ± 0.02
N37	2647.4 ± 1.4	-3.44 ± 0.28
N39	2776.6 ± 1.1	-1.31 ± 0.04
N42	2831.0 ± 0.2	-1.21 ± 0.03
N68	3627.7 ± 0.6	-1.08 ± 0.05
N72	3845.5 ± 2.4	-2.04 ± 0.16
N79	4088.9 ± 0.4	-0.89 ± 0.03
N82	4155.1 ± 1.6	-2.06 ± 0.23
N83	4288.2 ± 2.1	-2.55 ± 0.51
N84	4289.8 ± 0.9	-1.05 ± 0.08
N90	4437.3 ± 1.5	-3.20 ± 0.44
Fixed t_0		
Name	$t_0(\text{JD}-2450000)$	α
N22	1964.3	-4.35 ± 0.17
N26	2145.5	-1.92 ± 0.04
N33	2321.4	-1.22 ± 0.02
N34	2447.5	-1.70 ± 0.06
N40	2798.6	-1.67 ± 0.03
N45	2908.3	-0.97 ± 0.03
N48	2971.4	-0.92 ± 0.01
N50	2985.3	-1.37 ± 0.04
N52	3003.3	-1.43 ± 0.03
N59	3304.4	-1.63 ± 0.32
N65	3408.4	-1.44 ± 0.10
N71	3813.3	-2.92 ± 0.22
N75	3980.5	-2.28 ± 0.15
N85	4298.5	-1.16 ± 0.05
N87	4299.5	-1.22 ± 0.11
N88	4339.6	-1.48 ± 0.40

38% to be S-class, 1% to be C-class, 4% to be O-class and 16% to be J-class in their sample.

5. Recurrent Novae

Recurrent novae are potential supernovae progenitors (Schaefer 2010). We compare the position of our nova candidates with the catalog by Pietsch et al. (2007); Pietsch (2010). We have found 4 recurrent novae candidates by selecting novae in the literature which are located within 1 arcsec to our nova candidates (see Table 6 and Fig. 11). Among the potential recurrent nova candidates N29 has 3 outbursts in 12 years, which would be an unprecedented short period. As pointed out by Henze et al. (2009), the outburst appears earlier in UV and $H\alpha$ than in the R -band which does not fit very well to the nova scheme. They thus suggest an alternative scheme, that this event could be a dwarf nova in the Milky Way. N19 has 4 outbursts detected so far. Because the short time separation between the first two outbursts, Sharov & Alksnis (1989) have doubted its nova nature and suggested it to be a U Gem type foreground Galactic dwarf nova. However, the spectroscopic observations of the 4th outburst in 2010 (Shafter et al. 2010) have confirmed it as a He/N spectroscopic class nova located in M31. In addition, Pietsch et al. (2010) have also reported the SSS turn-on ~ 15 days after the first optical detection in 2010.

Table 6. Recurrent Nova candidates

WeCAPP ID	RA	DEC	NAME	RA	DEC	Separation	Δ_{M31}
N02 (M31N-1997-10f)	00:42:52.35	+41:16:13.2	M31N-2008-08b	00:42:52.38	+41:16:12.9	0''54	1'50
N19 (M31N-2001-07b)	00:42:57.75	+41:08:12.3	M31N-1963-09c	00:42:57.73	+41:08:12.4	0''32	8'29
N19 (M31N-2001-07b)	00:42:57.75	+41:08:12.3	M31N-1968-09a	00:42:57.71	+41:08:11.9	0''72	8'29
N19 (M31N-2001-07b)	00:42:57.75	+41:08:12.3	M31N-2010-10e	00:42:57.76	+41:08:12.3	0''15	8'29
N29 (M31N-2001-12b)	00:42:39.59	+41:09:02.9	M31N-1997-11k	00:42:39.59	+41:09:02.9	0''00	7'12
N29 (M31N-2001-12b)	00:42:39.59	+41:09:02.9	M31N-2009-11b	00:42:39.61	+41:09:03.2	0''42	7'12
N83 (M31N-2007-07a)	00:43:04.05	+41:17:08.3	M31N-1990-10a	00:43:04.05	+41:17:07.5	0''80	3'82

Notes. We give the WeCAPP name, the positions (also see Fig. 4), the corresponding novae fulfilling the $1''0$ criterion, the separation and the distance from the center of M31 (Δ_{M31}).

To test how likely an uncorrelated nova is falling into the 1 arcsec area, we perform a test by using the upper-right quarter of our pointing F1, which has the highest M31 light contribution from the bulge and contains 42 novae. The ratio of the area occupied by the $1''0$ circle of these 42 novae to the total area of this quarter (300×300 arcsec²), implies the chance of an uncorrelated nova to coincide with an existing nova is low (1.5 : 1000). As most of the recurrent novae are not found in this quadrant (see Fig. 4 and Table 6), the chance of coincidence is even smaller for the majority of the recurrent nova candidates.

Note that we use stricter selection criteria to search for recurrent novae, thus we have less candidates than presented by Pietsch et al. (2007); Pietsch (2010).

Hachisu & Kato (2006) suggested that recurrent novae all bear the plateau light curve. However, in our light curve we did not detect evident plateaus. The main reason is we do not have comprehensive coverage of the light curves. Despite of the lack of highly sampled observation, it would be hard to find such plateaus because the light curves in R or I are contaminated by the bright emission lines. Hachisu et al. (2008) thus advocate observations in Strömgren y -band (centered at 547 nm) since it is designed to cut the strong emission lines in the wide V band-pass filter and can follow the continuum flux more accurately. However, the Strömgren y -filter is narrow and requires longer exposure time, so we use the I -filter instead of the Strömgren y -filter for the confirmation of microlensing event from achromaticity when the WeCAPP was initiated.

6. Rate of decline and the speed class

In this section we present the rate of decline for our nova sample. Due to the observing gaps before some of the apparent maxima, it is hard to recover the true maximum fluxes during the nova eruption. Nevertheless, the apparent maxima can serve as a lower limit of the true maxima. One can derive upper limits for the t_2 values (the time required for the nova to faint by two magnitudes) if the apparent maxima are taken as the true maxima. We have retrieved the t_2 values for our sample as follows: we perform a linear fitting on the decline part of each light curve and determine the rate of decline, dm/dt (in units of magnitude/day). We then use dm/dt to derive the t_2 value relative to the observed maximum magnitude for all the novae. The result is shown in Fig. 13. Besides the linear fitting, we also applied the universal decline law proposed by Hachisu & Kato (2006) to retrieve the t_2 value from the observed magnitude at the apparent maximum. This procedure can only be done for 30 S-class novae, because the fitting routine fails to find a

solution for other classes. The result is shown in Fig. 14. The reader should keep in mind, that Fig. 13 or 14 does not give the exact MMRD relation, but serves as an upper limit in the t_2 and lower limit in the magnitude.

As pointed out by Warner (1989), the value of dm/dt is also an indicator of the speed class. We thus use the dm/dt values of our sample to derive the frequency of different speed classes of nova in M31. A comparison of the dm/dt distribution in our sample to the novae presented by Darnley et al. (2004) is shown in Fig. 15, the two M31 samples agree rather well within the statistical errors (shown are only the \sqrt{n} number count errors). The Milky Way data set of Stroepe et al. (2010) differs significantly by presenting a much higher fraction of very fast novae than the M31 data. For a fair comparison, one would have to correct the Stroepe et al. (2010) sample for its severe observational selection effects as being observed from inside the (dusty) Milky Way disk. A more detailed comparison is beyond the scope of this paper as it requires detailed modeling of the distribution of stellar and dust population of both galaxies.

7. Conclusion and outlook

We have presented the position, outburst time and the maximum brightness of the 91 nova candidates discovered during the time span of the WeCAPP project. Light-curve classifications under the taxonomic scheme of Stroepe et al. (2010) have been shown and the full R and I -band light curves of each individual nova during the outburst are also presented in the Appendix.

In this work we successfully applied a scheme developed for a Milky Way nova sample which, because of observational selection effects, is certainly dominated by the galactic disk, to a nova sample of a different host galaxy which is mostly observed towards the bulge of this host. The differences in member ratios for the subclasses as defined by Stroepe et al. (2010) between the Milky Way and our M31 WeCAPP sample probably reflect to some extent different observational selection effects, but bear the potential for further conclusions on the differences between stellar populations in M31 and the Milky Way, once the selection effects are properly accounted for.

We provide the full light curve data of the novae on request, as well as the postage stamps of the reduced, stacked, or difference-imaging frames.

Part of this catalogue has been used to find the X-ray counter-part by Pietsch et al. (2005, 2007) and showed that super soft X-ray sources (SSS) in M31 are mostly constituted by the novae during eruption. The turn on and turn off of the SSS phase provide us the information of the

Table 7. Speed class of nova according to Warner (1989)

Speed class	t_2 [day]	dV/dt [mag/day]	M31 sample		MW sample
			This work	Darnley et al. (2004)	Strope et al. (2010)
Very fast	≤ 10	≥ 0.2	8	1	35
Fast	11-25	0.18-0.08	18	3	27
Moderately Fast	26-80	0.07-0.025	46	11	23
Slow	81-150	0.024-0.013	11	2	7
Very slow	151-250	0.013-0.008	7	3	3
		≤ 0.08	1	0	2

ejected and accreted mass onto the surface of the white dwarf.

Besides the X-ray monitoring campaign, there is also a survey of M31 novae in infrared using *Spitzer Space Telescope* (Shafter et al. 2011a), which indicates a correlation between the dust formation timescales and the nova speed class. Such studies would not be possible without the speed class determined by the optical observations. Ground-based optical surveys, such as PTF (Law et al. 2009; Rau et al. 2009), PanSTARRS (Kaiser et al. 2002) and LSST (Tyson 2002), will continue to play an important role in the regime of multi-wavelength novae observation and help us to gain insight of the underlying physical mechanism of novae.

Acknowledgements. We are grateful for the comments from the anonymous referee. We thank Sara Bühler and Silona Wilke for their contributions in observation. This work was supported by the DFG cluster of excellence ‘Origin and Structure of the Universe’ (www.universe-cluster.de).

References

- Alard, C. & Lupton, R. H. 1998, *ApJ*, 503, 325
An, J. H., Evans, N. W., Hewett, P., et al. 2004, *MNRAS*, 351, 1071
Ansari, R., Aurière, M., Baillon, P., et al. 2004, *A&A*, 421, 509
Arp, H. C. 1956, *AJ*, 61, 15
Bianchini, A., Friedjung, M., & Brinkmann, W. 1992, *A&A*, 257, 599
Bode, M. F., Darnley, M. J., Shafter, A. W., et al. 2009, *ApJ*, 705, 1056
Calchi Novati, S., Covone, G., de Paolis, F., et al. 2007, *A&A*, 469, 115
Calchi Novati, S., Dall’Ora, M., Gould, A., et al. 2010, *ApJ*, 717, 987
Ciardullo, R., Ford, H. C., Neill, J. D., Jacoby, G. H., & Shafter, A. W. 1987, *ApJ*, 318, 520
Ciardullo, R., Shafter, A. W., Ford, H. C., et al. 1990, *ApJ*, 356, 472
Csák, B., Kiss, L. L., Retter, A., Jacob, A., & Kaspi, S. 2005, *A&A*, 429, 599
Darnley, M. J., Bode, M. F., Kerins, E., et al. 2006, *MNRAS*, 369, 257
Darnley, M. J., Bode, M. F., Kerins, E., et al. 2004, *MNRAS*, 353, 571
della Valle, M. & Livio, M. 1995, *ApJ*, 452, 704
Fliri, J., Riffeser, A., Seitz, S., & Bender, R. 2006, *A&A*, 445, 423
Gössl, C. A. & Riffeser, A. 2002, *A&A*, 381, 1095
Hachisu, I. & Kato, M. 2006, *ApJS*, 167, 59
Hachisu, I. & Kato, M. 2009, *ApJ*, 694, L103
Hachisu, I., Kato, M., Kiyota, S., et al. 2008, in *Astronomical Society of the Pacific Conference Series*, Vol. 401, RS Ophiuchi (2006) and the Recurrent Nova Phenomenon, ed. A. Evans, M. F. Bode, T. J. O’Brien, & M. J. Darnley (ASP, San Francisco), 206
Henze, M., Pietsch, W., Haberl, F., et al. 2010a, *A&A*, 523, A89
Henze, M., Pietsch, W., Haberl, F., et al. 2010b, *ArXiv e-prints*
Henze, M., Pietsch, W., Haberl, F., et al. 2010c, *Astronomische Nachrichten*, 331, 193
Henze, M., Pietsch, W., Podigachoski, P., et al. 2009, *The Astronomer’s Telegram*, 2286, 1
Hubble, E. P. 1929, *ApJ*, 69, 103
José, J. & Hernanz, M. 2007, *Journal of Physics G Nuclear Physics*, 34, 431
Joshi, Y. C., Pandey, A. K., Narasimha, D., et al. 2004, *A&A*, 415, 471
Kaiser, N., Aussel, H., Burke, B. E., et al. 2002, in *Presented at the Society of Photo-Optical Instrumentation Engineers (SPIE) Conference*, Vol. 4836, Society of Photo-Optical Instrumentation Engineers (SPIE) Conference Series, ed. J. A. Tyson & S. Wolff (SPIE, Bellingham), 154–164
Kato, T., Nakajima, K., Maehara, H., & Kiyota, S. 2009, *ArXiv e-prints*
Law, N. M., Kulkarni, S. R., Dekany, R. G., et al. 2009, *PASP*, 121, 1395
Livio, M. 1992, *ApJ*, 393, 516
Lynch, D. K., Woodward, C. E., Gehrz, R., et al. 2008, *AJ*, 136, 1815
McLaughlin, D. B. 1945, *PASP*, 57, 69
Orio, M. 2006, *ApJ*, 643, 844
Payne-Gaposchkin, C. 1964, *The galactic novae*, ed. Gaposchkin, C. H. P. (Dover, New York)
Pejcha, O. 2009, *ApJ*, 701, L119
Pietsch, W. 2010, *Astronomische Nachrichten*, 331, 187
Pietsch, W., Fliri, J., Freyberg, M. J., et al. 2005, *A&A*, 442, 879
Pietsch, W., Haberl, F., Sala, G., et al. 2007, *A&A*, 465, 375
Pietsch, W., Henze, M., Haberl, F., & Burwitz, V. 2010, *The Astronomer’s Telegram*, 3038, 1
Rau, A., Kulkarni, S. R., Law, N. M., et al. 2009, *PASP*, 121, 1334
Rector, T. A., Jacoby, G. H., Corbett, D. L., & Denham, M. 1999a, in *Bulletin of the American Astronomical Society*, Vol. 31, Bulletin of the American Astronomical Society, 1420–1421
Rector, T. A., Jacoby, G. H., Corbett, D. L., Denham, M., & RBSE Nova Search Team. 1999b, in *American Astronomical Society Meeting Abstracts*, Vol. 195, American Astronomical Society Meeting Abstracts, 36.08
Riffeser, A., Fliri, J., Bender, R., Seitz, S., & Gössl, C. A. 2003, *ApJ*, 599, L17
Riffeser, A., Fliri, J., Gössl, C. A., et al. 2001, *A&A*, 379, 362
Riffeser, A., Seitz, S., & Bender, R. 2008, *ApJ*, 684, 1093
Rosino, L. 1964, *Annales d’Astrophysique*, 27, 498
Rosino, L. 1973, *A&AS*, 9, 347
Rosino, L., Capaccioli, M., D’Onofrio, M., & della Valle, M. 1989, *AJ*, 97, 83
Schaefer, B. E. 2010, *ApJS*, 187, 275
Shafter, A. W. 1997, *ApJ*, 487, 226
Shafter, A. W., Bode, M. F., Darnley, M. J., Ciardullo, R., & Misselt, K. A. 2010, *The Astronomer’s Telegram*, 3006, 1
Shafter, A. W., Bode, M. F., Darnley, M. J., et al. 2011a, *ApJ*, 727, 50
Shafter, A. W., Darnley, M. J., Hornoch, K., et al. 2011b, *ArXiv e-prints*
Shafter, A. W. & Irby, B. K. 2001, *ApJ*, 563, 749
Shara, M. M. 1981, *ApJ*, 243, 926
Sharov, A. S. & Alksnis, A. 1991, *Ap&SS*, 180, 273
Sharov, A. S., Alksnis, A., Zharova, A. V., & Shokin, Y. A. 2000, *Astronomy Letters*, 26, 433
Sharov, A. S. & Alksnis, A. K. 1989, *Soviet Astronomy Letters*, 15, 382
Simon, V., Hornoch, K., Kušnirák, P., Šarounová, L., & Wolf, M. 2005, in *Astronomical Society of the Pacific Conference Series*, Vol. 330, *The Astrophysics of Cataclysmic Variables and Related Objects*, ed. J.-M. Hameury & J.-P. Lasota (ASP, San Francisco), 449
Strope, R. J., Schaefer, B. E., & Henden, A. A. 2010, *AJ*, 140, 34
Tanaka, J., Nogami, D., Fujii, M., Ayani, K., & Kato, T. 2010, *ArXiv e-prints*
Tomaney, A. B. & Shafter, A. W. 1992, *ApJS*, 81, 683
Tyson, J. A. 2002, in *Presented at the Society of Photo-Optical*

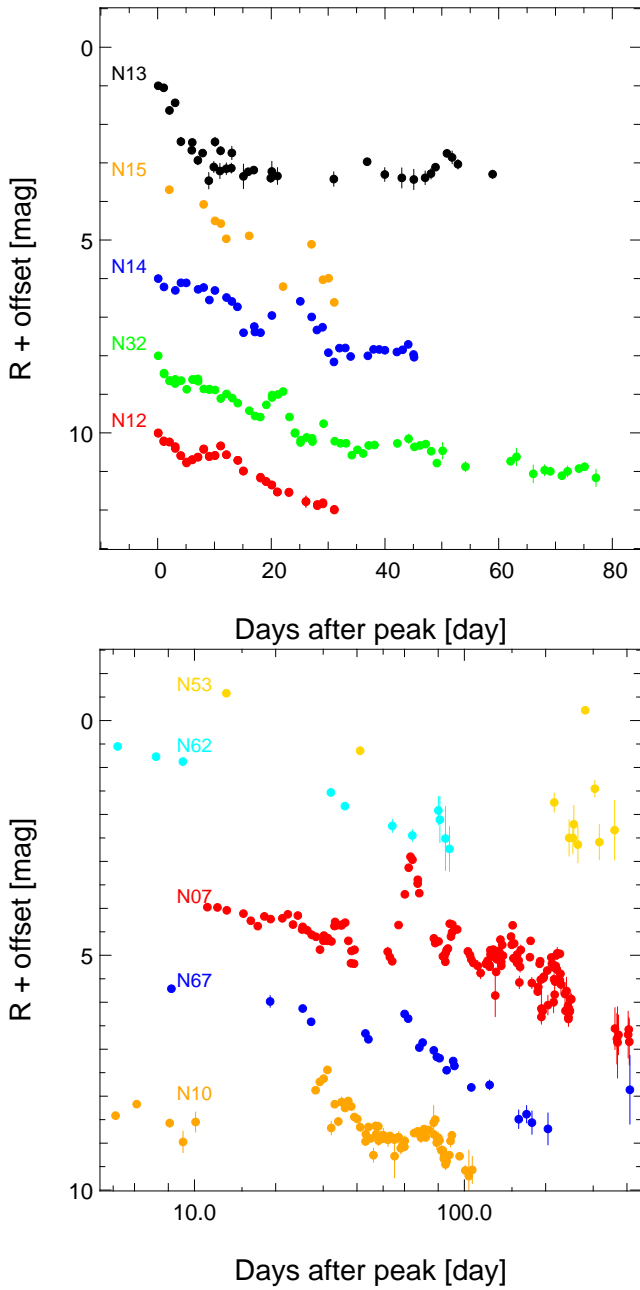


Fig. 7. C Class novae. The offsets applied to the magnitudes are -15.07 for N07, -11.88 for N10, -8.26 for N12, -17.71 for N13, -11.58 for N14, -13.79 for N15, -9.16 for N32, -19.19 for N53, -19.15 for N62 and -13.04 for N67 respectively. Here we only show the decline part of the light curve. Full light curves can be found in the appendix.

Instrumentation Engineers (SPIE) Conference, Vol. 4836, Society of Photo-Optical Instrumentation Engineers (SPIE) Conference Series, ed. J. A. Tyson & S. Wolff (SPIE, Bellingham), 10–20
 Warner, B. 1989, in *Classical Novae*, ed. M. F. Bode & A. Evans (Cambridge Univ. Press, Cambridge), 1–16
 Williams, R. E. 1992, *AJ*, 104, 725
 Zwicky, F. 1936, *PASP*, 48, 191

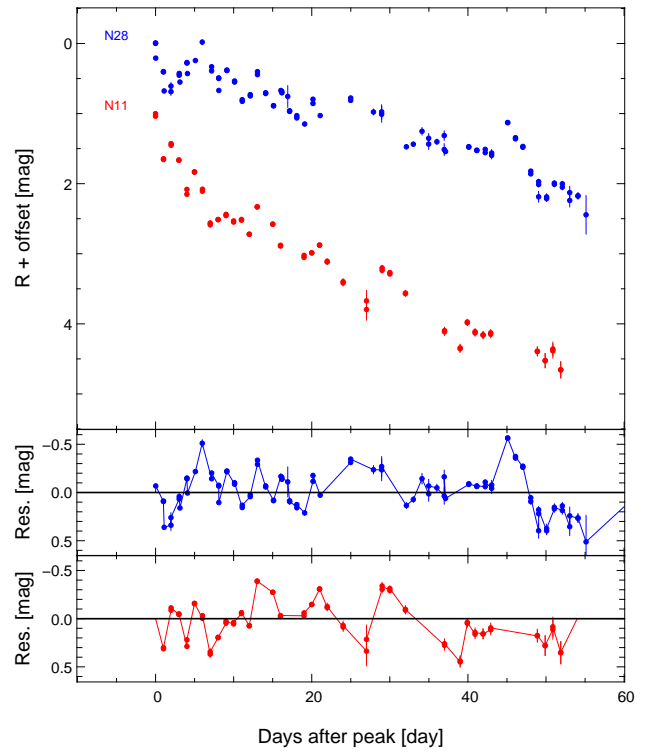


Fig. 8. O Class novae. The offset is -15.77 for N11 and -17.61 for N28 respectively. Here we only show the decline part of the light curve. Full light curves can be found in the appendix.

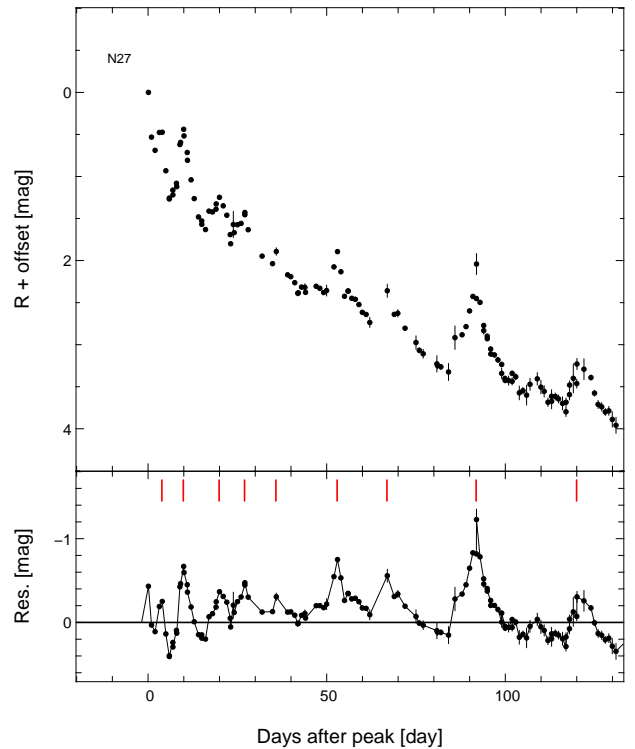


Fig. 9. J Class nova. The single offsets are -16.99 for N27. Here we only show the decline part of the light curve. Full light curves can be found in the appendix.

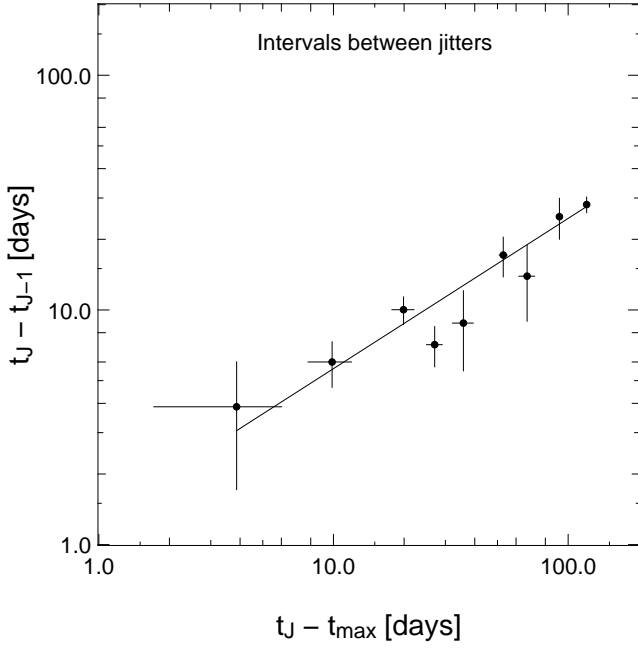


Fig. 10. J-class peak intervals for nova N27, using *R*-band data.

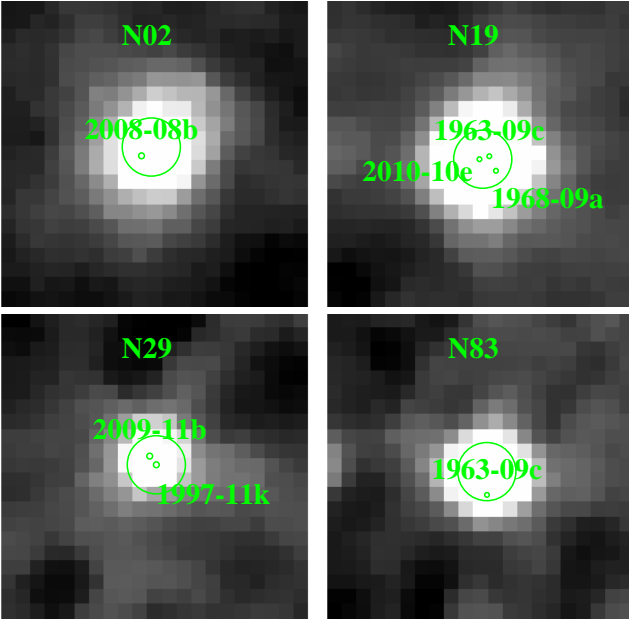


Fig. 11. Position of the recurrent. The larger circle in the center indicates the $1''$ radius for our selection criteria. The position of potential recurrent nova candidates are marked by the smaller circles.

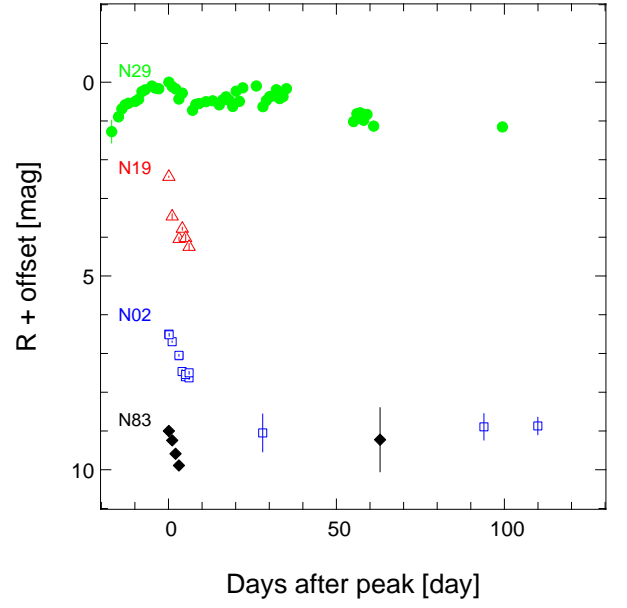


Fig. 12. Recurrent nova candidates light curves. The single offsets are -11.76 for N02, -16.76 for N19, -18.86 for N29 and -9.86 for N83 respectively. Here we only show the decline part of the light curve. Full light curves can be found in the appendix.

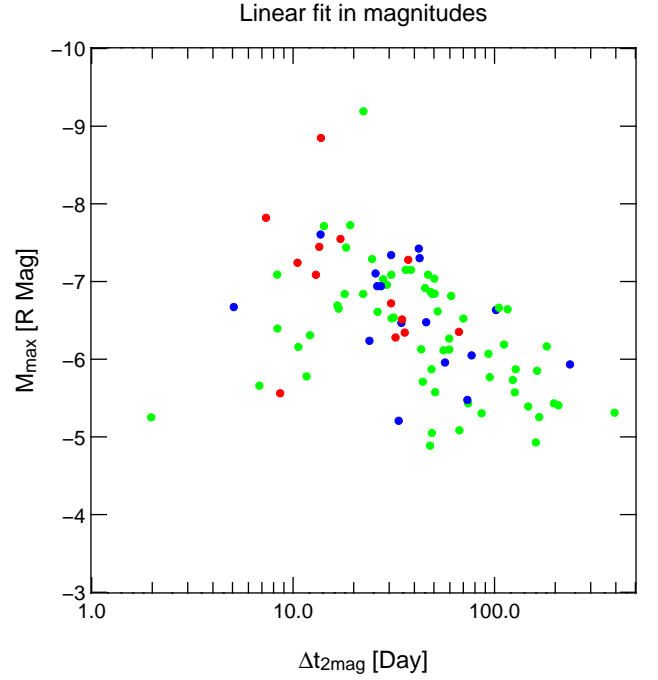


Fig. 13. Distribution of the observed apparent maximum brightness in *R*-band and the fitted t_2 for all nova candidates. The red and blue points are referred to equation (3) with t_0 as free parameter and equation (4) with t_0 as fixed parameter, respectively. The green points are novae belong to other classes. The t_2 value is derived from the dm/dt and the observed apparent maximum in the light curves. See the main text for detailed description.

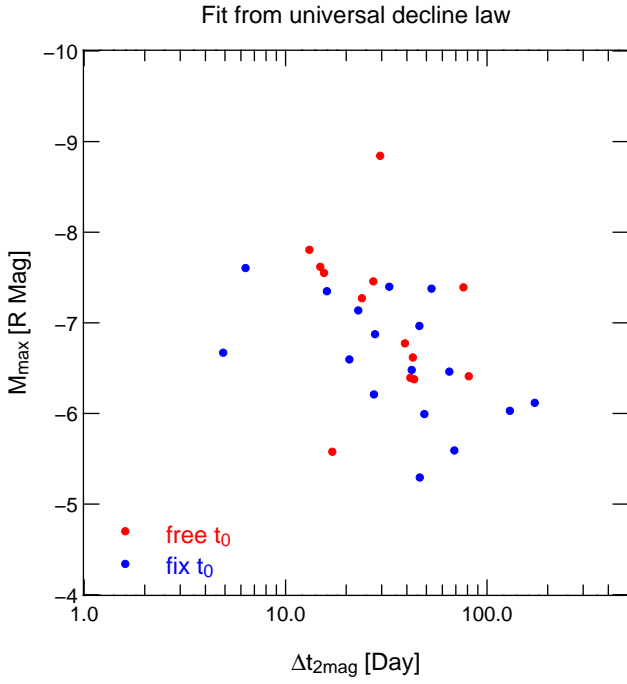


Fig. 14. Distribution of the observed apparent maximum and the fitted t_2 for S-class novae. The t_2 value is derived from the universal decline law (Hachisu & Kato 2006) and the observed apparent maximum in the light curves. See the main text for detailed description. The red and blue points are referred to equation (3) with t_0 as free parameter and equation (4) with t_0 as fixed parameter, respectively.

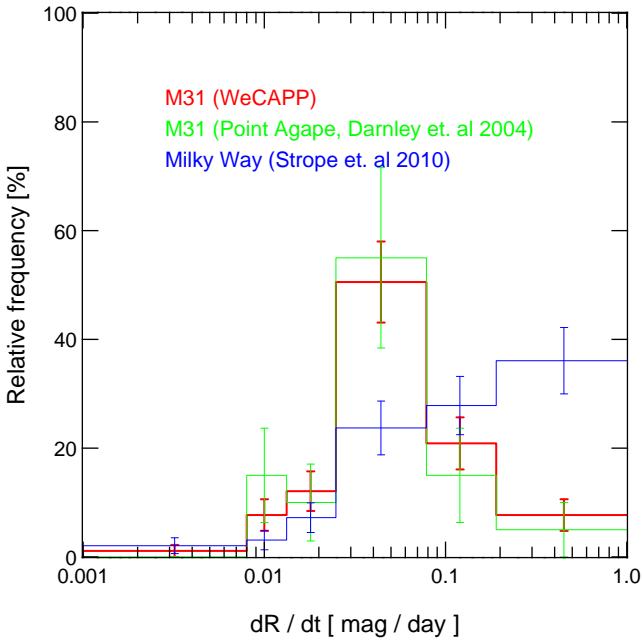


Fig. 15. The distribution of the speed class of novae in M31 (see Table 7, for definition see Warner (1989)). The red line is derived from our sample and the green line is from the M31 novae presented by Darnley et al. (2004). The blue line represents the Milky Way novae by Strope et al. (2010).